# SAFETY OF METALLIC IMPLANTS IN MAGNETIC RESONANCE IMAGING

A THESIS

SUBMITTED TO THE DEPARTMENT OF ELECTRICAL - ELECTRONICS ENGINEERING

AND THE INSTITUTE OF ENGINEERING AND SCIENCE

OF BILKENT UNIVERSITY

IN PARTIAL FULFILLMENT OF THE REQUIREMENTS

FOR THE DEGREE OF

MASTER OF SCIENCE

By

Onur Ferhanoğlu

November, 2005

I certify that I have read this thesis and that in my opinion it is fully adequate, in scope and in quality, as a thesis for the degree of Master of Science.

Prof. Dr. Ergin Atalar(Supervisor)

I certify that I have read this thesis and that in my opinion it is fully adequate, in scope and in quality, as a thesis for the degree of Master of Science.

Assist. Prof. Dr. Vakur B. Ertürk

I certify that I have read this thesis and that in my opinion it is fully adequate, in scope and in quality, as a thesis for the degree of Master of Science.

Prof. Dr. Nevzat Gencer

Approved for the Institute of Engineering and Science:

Prof. Dr. Mehmet Baray
Director of the Institute Engineering and Science

# ABSTRACT

## SAFETY OF METALLIC IMPLANTS IN MAGNETIC RESONANCE IMAGING

Onur Ferhanoğlu
M.S. in Electrical - Electronics Engineering
Supervisor: Prof. Dr. Ergin Atalar
November, 2005

Magnetic Resonance Imaging (MRI) is safe only if we take safety precautions. In the presence of a metallic implant inside the body, three types of magnetic fields encountered in MRI (Static magnetic field, radiofrequency field, gradient field) may become the sources of safety problems. In this thesis, temperature increase created by a pacemaker under MRI is investigated. Electromagnetic simulations are performed, in-vivo, phantom experiments are conducted and finally bioheat equation is solved to find the corresponding temperature increase. Using this temperature increase the input power can be limited to ensure safe scans. MRI compatible lead design is the essential innovation of this thesis which is directly applicable to any kind of metallic, wire shaped interventional MRI device.

*Keywords:* Magnetic Resonance Imaging, metallic implant, pacemaker, bioheat transfer, interventional MRI.

# ÖZET

# MANYETİK REZONANS GÖRÜNTÜLEMEDE METALİK İMPLANTLARIN GÜVENLİĞİ

Onur Ferhanoğlu
Elektrik - Elektronik Mühendisliği, Yüksek Lisans
Tez Yöneticisi: Prof. Dr. Ergin Atalar
Kasım, 2005

Manyetik resonans görüntüleme (MRG), güvenli olduğu bilinen bir teşhis yöntemidir. Ancak metal bir implantın varlığında, MRG'de karşılaşılan manyetik alanlar (Sabit manyetik alan, radyofrekans alanı, gradyan manyetik alan) güvenlik problemlerinin kaynagı olabilmektedir. Bu tezde, MRG esnasında kalp pilinin ne kadar sicaklık artışına sebebiyet verebileceği araştırılmıştır. Bu artışı bulmak için, Elektromanyetik simülasyonlar yapılmış, in-vivo, phantom deneyleri gerçekleştirilmiş ve son olarak bioısı denklemi çözülmüştür. Bu tezin getirdiği esas yenilik, MRG uyumlu kalp pili kablosu tasarımıdır. Bu tasarımnı aynı zamanda metalik, kablo şeklinde olan bütün girişimsel MRG cihazlarına da uygulanabilirliği mevcuttur.

*Anahtar sözcükler*: Manyetik Rezonans Görüntüleme, metal implant, kalp pili, bioısı transferi, Girişimsel Manyetik Rezonans Görüntüleme.

# Acknowledgement

Upon the completion of this thesis, I would like to express my gratitude to all those who have contributed. First of all, I would like to thank Prof. Dr. Ergin Atalar for his great supervision. He has provided me opportunities that I could never have imagined of.

Yiğitcan Eryaman, Onur Taşcı, Levent Özparlak, Halise Irak and Sinem Güravşar, Imran Akċa actively contributed the experiments I've conducted. Without them it would have been impossible.

I have been a visiting researcher at Johns Hopkins University School of Medicine on July 2004. During my time there, AbdelMonem M. El-Sharkawy has helped me very much, I would like to thank him for his kind support.

I'd also like to thank, Prof. Dr. Ayhan Altıntaş, Assist. Prof. Dr. Vakur Ertürk, Özgür Salih Ergül, Haydar Ċelik, Onur Afacan and Gökalp Memiş for the useful discussions. I thank Prof. Dr. Nevzat Gencer for taking part in my jury.

I've performed animal experiments at Başkent University. I'd like to thank Dr. Hale Tufan and Dr. Didem Bacanlı for sharing their lab and assisting me in the experiments.

Finally thanks should be given to my parents for motivating me which made it possible to complete this work.

*To those implanted with pacemakers*

# Contents

# List of Figures

# List of Tables

# Chapter 1

# Introduction

## 1.1 Motivation

An artificial pacemaker is a signal generator for the heart. It is needed when heart's natural pacemaker is no longer functioning properly. In the United States, there are approximately 750,000 patients with cardiac pacemakers or implantable cardioverter defibrillators (ICDs) [1], and this number is growing. Among these patients, 60,000 require a Magnetic Resonance Imaging (MRI) examination every year . These numbers are representative for the rest of the world as well. Unfortunately, current pacemaker and ICDs are not compatible with MRI and therefore the patients with pacemakers are denied from MRI examination. Therefore they receive suboptimal healtcare. If the pacemaker and ICDs can be made MRI compatible, the physicians can apply state of art diagnostic procedures to the patients without limitations. [1]

Safety issues, related to cardiac pacemakers and ICDs are; the possibility of dislocation of the pacemaker due to static magnetic field, the possibility of undesired pacing of the heart by the induced currents to the pacing leads, the

[1]There are 750,000 people in U.S that are implanted with pacemakers [1]. 30,000,000 people have gone under MRI scan in 2004 [2], which is 1/8 the population in U.S. Therefore 60,000 patients with pacemakers are expected to go under MRI scan per year.

possibility of causing malfunction in the electronic circuit of the pulse generator due to interference from the MRI electromagnetic field, the possibility of changing the mode of the pacemaker by causing the switching on/off of the reed relays in the implant; and finally the possibility of excessive heating around the implant due to the concentration of the electromagnetic field around the pacemaker.

The purpose of this thesis is to first investigate heating and temperature increase caused by the device and finally to provide a solution that would prevent such an increase in temperature.

## 1.2 Literature Review

Many cases with substantial temperature increase of metallic implants were reported and reviewed [3]. Also there are several designs and solutions to this problem provided by scientists, which will be summarized below.

Achenbach et. al. [4] reported a maximum temperature increase of 63.1 $^oC$ during 90 seconds of scanning, additionally in an in vitro evaluation of 44 commercially available pacemaker leads, Sommer et al. [5] observed a temperature increase of 23.5 $^oC$ at 0.5 tesla experiment. Substantial temperature increase were also observed in a previous study by Gleason et al. regarding the effect of MRI on Deep Brain Stimulators (DBSs), a device, composed of a case and leads (similar to the pacemaker) for the treatment of essential tremor and Parkinson's tremor. [6]. Furthermore at 1.5 T and a Specific Absorbtion Rate (SAR) of 3.0 W/kg have been shown to cause severe necrosis in the mucous membranes of dogs with transesophageal cardiac pacing leads [7].

Smith et al. observed 16.8 $^oC$ temperature increase on a half wavelength wire in a gel-phantom experiment [8, 9]. Konings et al. observed temperature increases due to endavascular guidewires between 26 $^oC$ and 74 $^oC$ in saline bath experiments up to 30 seconds of scan time [10]. In another experiment with saline solution up to 34 $^oC$ of temperature increase was observed for a half wavelength wire [10]. First, second or third order burns were observed in in-vivo studies

mentioned above [4, 8, 9, 10, 11, 12].

A recent study was performed for one of the most widely used neurostimulation system (Activa Tremor Control System, Medtronic). Different configurations were evaluated to asses worst case and clinically relevant positioning scenarios [13]. In vitro experiments were performed at 64MHz MR system using gel phantoms to represent human tissue. The highest temperature change observed was 25.3 $^oC$ for the RF coil and 7.1 $^oC$ for the head coil. These results indicate that heating may be hazardous under certain conditions.

The FREEHAND System Implantable Functional Neurostimulator (FNS) (NeuroControl, Cleveland, OH) is an RF-powered motor control neuroprosthesis that consists of both implanted and external components [14]. Findings from of an MRI-induced heating experiment during which the FREEHAND System was exposed to a whole-body-averaged SAR of 1.1 W/kg for 30 minutes showed that localized temperature increases were no greater than 2.7 $^oC$ with the device in a gel-filled phantom. A patient with a FREEHAND system can only undergo MR procedure under certain input power levels for 1.5 Tesla scanner.

Several strategies may be used to ensure safety in metallic implants. One of the basic ones is to limit the input RF power as it may required for the above mentioned FREEHAND system. Seeking for a power threshold that ensures reasonable amount of heating is a meaningful approach. A methodology for such a power limitation was previously published [15]. Many modern pulse sequences such as fast spin-echo or steady-state free precession (SSFP) requires high RF power levels and therefore there is no guarantee that good quality images can be acquired with this limitation.

Most of the studies on the heating of metallic implants concentrates on the heating of the leads rather than generator. Generator, as a smooth device with curved edges is a less threatening structure than the leads in terms of electromagnetic field concentration, therefore less heating is observed and smaller temperature increase is expected [16, 17]. The safe coaxial cable design [18] is a design based on the modification of the lead with a special coaxial cable. In the design, RF chokes are used in between every quarter wavelength. However in

the safe coaxial design, high permittivity materials needs to be employed. This may create flexibility problems since high permittivity materials are brittle and rigid. There may be more than one the lead which may require usage of separate coaxial cables. In such a case miniaturization of the design is a difficult task.

RF chokes and filters were used in several previous studies. Susil et al [19] used RF chokes in the design of a combined electrophysiology/MRI catheter. Ladd et. al. [20] used triaxial chokes to present a high impedance to currents flowing on the outer surface of the triaxial cable. Medtronics developed an implantable medical device incorporating integrated circuit notch filters [21], and Telectronics developed pacemaker with Electromagnetic Interference (EMI) protection [22]. Both of the designs ensure electromagnetic interference is not a problem however safety in terms of heating is not guaranteed. High current may still be flowing through long cables and these high currents may cause excessive heating and burns. Optical signal transmission in between the generator and the organ, such as Biophan's "photonic pacemaker" [23], provides safety [24], since there is no coupling with the optical system and the electromagnetic field, however the electrical to optical and optical to electrical energy conversion efficiency is limited and therefore the lifetime of the pulse generator reduces significantly. The miniaturization is also difficult task.

In the studies mentioned above various experimental methods were used. In some of them in-vivo data has been published, however in others temperature increase in gel and saline phantom studies were given. Since perfusion does not exist in gel phantom studies, these experiments are not valid indicators of the in-vivo temperature increase due to an implant. Also in saline phantoms convectional water flow occurs, which is a non-valid indicator as well. These problems created some variability between in-vivo and phantom studies and therefore reduced the trust in these studies. Recently a methodology was proposed to eliminate such discrepancies [15]. According to this study an electromagnetic simulation of the implant inside the body is performed and the amplification of the SAR due to the implant is compared with the corresponding phantom experiment. After such a verification, the SAR distribution of a body with the implant is convolved

with the Green's Function of the bioheat equation [25] to obtain the corresponding in-vivo temperature increase. Convolving SAR distribution with the Green's function has a low pass filtering effect. In other words, the temperature distribution is a smoothed and scaled version of the SAR distribution. Since temperature is a better indicator of tissue damage, this method should be obeyed in phantom studies for determining an input power threshold for the implant that would cause no damage on the patients. Every implant is safe if the input power threshold is correctly adjusted.

The proposed design in this thesis will enable patients that are implanted with metallic devices to be scanned under MRI with normal operating conditions of 8 W/kg spatial peak SAR at 1.5 T [26], without the restrictions of other safety approaches listed above.

## 1.3 Organization of the Thesis

This thesis is organized in the following order: Chapter 2 dwells upon the basic theory of radio frequency heating. In Chapter 3, Methods and Materials are discussed. Electromagnetic simulations, experiments and solutions to the bioheat equation are being emphasized. The results are given in Chapter 4 and finally Chapter 5 concludes the thesis. Some work on other safety issues are discussed in Appendix section.

# Chapter 2

# Theory

## 2.1 RF heating in MRI

The United States Food and Drug Administration (FDA) considers an MRI exam safe either if SAR does not exit 8 W/kg in the head and trunk , 12 W/kg in the extremities when averaged over a gram of tissue for 15 minutes or temperature changes do not exceed 1 $^oC$ in the head, 2 $^oC$ in the trunk and 3 $^oC$ in the extremities [26] . However no relationship is provided between SAR and temperature by this FDA guidelines. Both SAR and temperature are important measures. SAR can be measured with a phantom experiment, in which a phantom with electromagnetic properties similar to a human being is used. On the other hand temperature depends on the thermal characteristics of the tissue and perfusion which is the amount of blood volume in milliliters per 100 grams of tissue per minute. Perfusion is not easily simulated in a phantom. Therefore temperature for in vivo experiments should be reported [25].

Temperature can be found from SAR using below scheme that was proposed in a previous study [15]. According to this scheme, power that is transmitted through the transmit coil is deposited inside the tissue due to conductive losses. The first system is modelled with Maxwell's equations to find the electric field. SAR is given by:

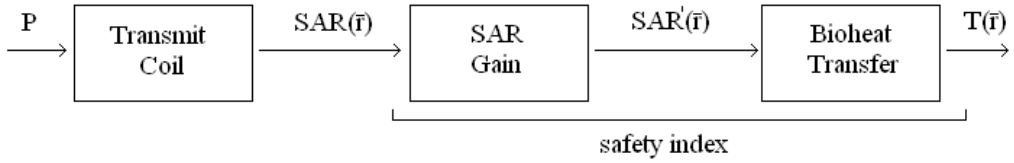


Figure 2.1: RF heating scheme: Power, transmitted by the RF coil is absorbed by the tissues, denoted as the specific absorbtion rate (SAR). Existence of a metallic implant causes an amplification in the local SAR, and the resultant distribution is denoted as SAR'. This amplification creates temperature increase, which is modelled by bioheat transfer equation. Safety index is the temperature increase per unit SAR applied ($^oC/(\mathrm{W/kg})$) and can be used to set limits on the spatial peak SAR [15].

$$SAR = \frac{\sigma E^2}{\rho_t} \tag{2.1}$$

where $E$ is the root mean square value of the electric field, $\sigma$ is the electrical conductivity at 64 Mhz (1.5 Tesla) and $\rho_t$ is the tissue mass density.

The second system is modelled with bioheat transfer equation [27]:

$$\frac{1}{\alpha}\frac{d\Delta T(r,t)}{dt} = \nabla^2 \Delta T(r,t) - v^2 \Delta T(r,t) + \frac{\rho_t}{k} SAR'(r,t) \tag{2.2}$$

where $\alpha$, $v$, $k$, $\Delta T$ are the thermal diffusivity, lumped perfusion, thermal conductivity and temperature increase with respect to base line respectively.

$v$ is directly proportional with perfusion, $m$, and is given by:

$$v = \sqrt{\frac{\rho_t \rho_b c_b m}{k}} \tag{2.3}$$

where $\rho_b$, $c_b$ are mass density of blood, specific heat capacity of blood respectively. And the laplacian operator in cartesian coordinates is given by:

$$\nabla^2 T = \frac{\partial^2 T}{\partial x^2} + \frac{\partial^2 T}{\partial y^2} + \frac{\partial^2 T}{\partial z^2} \tag{2.4}$$

Laplacian term in bioheat equation accounts for conduction in the heat transfer. Such a transfer occurs due to spatial differences in a thermal distribution.

When local heating is considered, in other terms when thermal parameters ($\alpha$, $v$, $k$) are constant in the local region of interest and if this local region is small with respect to whole body, not near the surface (infinite boundary condition) the bioheat equation can be treated as a linear shift-invariant system. This way, the system is fully characterized by its Green's function [25].

Green's functions, G, of the tissue bioheat equation in cylindrical (line source) and spherical (point source) coordinates are listed below. R is the distance from point source, r is distance from line source; t is time and $K_0$ is the modified Bessel function of the second kind and order zero [25].

Steady state cylindrical:

$$G_c(r) = \frac{\rho_t}{2\pi k} K_0(vr) \tag{2.5}$$

Steady state spherical:

$$G_s(R) = \frac{\rho_t}{4\pi k R} e^{-vR} \tag{2.6}$$

Time-dependent cylindrical

$$G_{ct}(r,t) = \frac{\rho_t}{4\pi k t} e^{-(r^2/4\alpha t)} e^{-\alpha v^2 t} \tag{2.7}$$

Time-dependent spherical

$$G_{st}(R,t) = \frac{\alpha \rho_t}{k(4\pi\alpha t)^{3/2}} e^{-(R^2/4\alpha t)} e^{-\alpha v^2 t} \tag{2.8}$$

Using above functions it is possible to find temperature increase for either a point source or a cylindrical source. The next section will develop further theory on Green's functions and introduce a method to predict in-vivo steady state temperature increase using a phantom.

## 2.2 Simulating perfusion in a perfusionless phantom

There are difficulties in conducting in vivo experiments: Exposing human to potentially unsafe environment cannot be justified. Using animals in such experiments may lead to error since perfusion levels in animals are not necessarily in the same level as humans. In this subsection, an easy way of predicting in-vivo steady state temperature increase will be described.

The steady-state temperature rise in a perfused body is always smaller than the steady-state temperature rise in a perfusionless phantom since perfusion dissipates heat. Therefore, when measuring the temperature on a phantom, there will be a time point that the phantom temperature would be equal to the perfused body steady-state temperature value. An analysis was performed showing that this time point is always very close to the perfusion time constant, which is :

$$1/\alpha v^2 \tag{2.9}$$

As previously mentioned, the bioheat equation can be solved by convolving the SAR distribution by the Green's function to yield the resulting temperature distribution, shown here for steady-state conditions [25]:

$$\Delta T_{ss}(\vec{r}_0) = \int SAR(\vec{r}) G_s(\vec{r} - \vec{r}_0) dV \tag{2.10}$$

$\Delta T_{ss}(\vec{r}_0)$ is the steady state temperature increase at $\vec{r}_0$ point. where the integral is performed over the whole volume, $V$ and $G$ is the Green's function [25] . The temperature at any position $\vec{r}_0$ , at steady state is a weighted average. For example, in the case of a spherically symmetric SAR distribution centered at the origin, this integral becomes:

$$\Delta T_{ss} = \int_0^\infty SAR(r) G_s(r) 4\pi r^2 dr \tag{2.11}$$

where r is the radius, $4\pi r^2$ is the Jacobian.

Spatial three-dimensional Fourier Transform of the Green's function in perfused tissue yields the following:

$$\mathbf{G}(\xi) = \frac{\rho_t}{kv^2} \frac{1}{1 + \frac{\xi^2}{v^2}} \tag{2.12}$$

where, $\xi$ is the spatial radial frequency variable of the Fourier transform.

On a perfusionless phantom with identical thermal conductivity and diffusion as in the in vivo case, the Green's function takes the following time dependent form [25]:

$$\mathrm{G_{st}(R,t)} = \frac{\alpha\rho_\mathrm{t}}{k\left(4\pi\alpha t\right)^{3/2}} \exp\left(-\frac{\mathrm{R}^2}{4\alpha t}\right) \tag{2.13}$$

which represents temperature distribution in phantom as a function of time when an impulse SAR is applied to a point at the center of a phantom.

When a unit step heating is applied to a point at the center of a phantom for a period of $\tau$, where $\tau$ is the perfusion time constant: $\tau = 1/(\alpha v^2)$, phantom temperature distribution can be found as:

$$G_p(r,\tau) = \int_0^\tau G_{st}(r,t)dt \tag{2.14}$$

In order to compare this perfusionless phantom temperature distribution with in vivo temperature distribution, we take the three-dimensional spatial Fourier transform of it:

$$G_p(\xi) = \frac{\rho_t}{kv^2} Q(\xi/v) \tag{2.15}$$

where

$$Q(\xi) = \frac{2}{\xi} \int_0^\infty \mathrm{erfc}(r) \sin(2\xi r)\, dr \tag{2.16}$$

where erfc is complimentary error function. As can be seen the coefficients of Equations 2.12 and 2.15 are identical and both depend only on the radial component of the frequency normalized with the lumped perfusion constant, v. The functions $Q(\xi)$ and $1/(1+\xi^2)$ are two very similar functions. The deviation in between these two spatial fourier transforms is always less than 30 percent. To find the temperature increase, these fourier transforms should be convolved with the SAR distribution.

$$T(\vec{r}_0) = \int SAR(\vec{r})G(\vec{r}-\vec{r}_0)dV \tag{2.17}$$

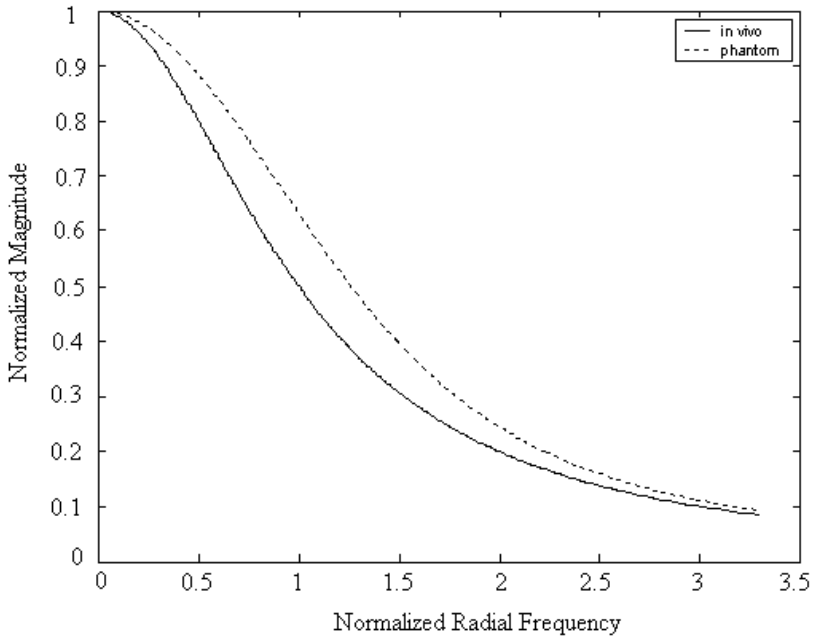


Figure 2.2: Comparison of Fourier transform of in vivo Green's function with phantom Green's function. Both X and Y axis are normalized

The above integral is basically the weighted average of the Green's function. If the functions $Q(\xi)$ and $1/(1+\xi^2)$ deviate by an amount of 30 percent at most, the result of the convolution is also bounded to 30 percent deviation.

Therefore, one can predict in vivo temperature increase from a phantom experiment. To do so, first of all a gel phantom that matches the geometric, electrical properties and the thermal conductivity of the tissue in which the metallic device

will be used has to be constructed. The electromagnetic part of the problem, particularly geometry, electrical permittivity, and electrical conductivity, must be properly simulated physically. In this thesis supermarket jell was used. Relative permittivity and conductivity were measured as described in the appendix section.

The temperature probe at the suspected spots must be appropriately positioned. The temperature rise at the time of perfusion time constant of the tissue should be reported. Values for perfusion time constants for some human tissues are shown in table 2.1 [15].

While doing an experiment on an implant, the SAR should be measured at the hot spot, highest heating point of the implant and at the same location with the implant removed for normalization purposes. In vivo temperature rise should be normalized with applied SAR. Certain geometric effects such as moving the phantom off center or changing the depth of the object in the phantom will change the absolute amount of heating measured near the device but this will be caused by a proportional change in the heating at the same location without the device in place. These effects can be accounted for with this normalization step.

Since the phantom possesses uniform thermal and electrical properties, above analysis is only valid for local heating rather than whole body heating. For this assumption to hold the size of the hot spot should be much smaller than the surrounding tissue and it should be far away from the boundary, not to encounter heat transfer with surrounding tissues. Often, the device will be placed in a variety of tissues. In such a case the worst case values (lowest perfusion and thermal conductivity) should be selected.

SAR should be reported in the phantom experiment so that the temperature increase at the hot spot, both in phantom and in-vivo measurements, is normalized with respect to same power level. Any temperature probe used to measure SAR in a phantom, no matter how small, will be unable to perform an ideal point measurement. Instead, it will have a sensitivity profile over which it performs a temperature average. This should be considered.

| Tissue Type | Perfusion (ml/100g/min) | Perfusion time constant (min) |
|---|---|---|
| Bone | 1.4 | 71 |
| Fat | 3.7 | 27 |
| Skin | 9.8-780 | 10.2-0.13 |
| Resting skeletal muscle | 1.9 | 37 |
| Skeletal muscle | 3.9-39 | 26-2.6 |
| Exercising skeletal muscle | 27 | 3.7 |
| Brain | 54 | 1.8 |
| Liver | 58 | 1.7 |
| Cardiac muscle | 83-600 | 1.2-0.17 |
| Kidney | 420 | 0.24 |

Table 2.1: Perfusion time constants for selected tissue types. [25]

## 2.3 RF Safety of wires in interventional MRI

In a previous work, which demonstrated RF heating scheme shown in Figure 2.3, insulated and noninsulated wire structures were numerically analyzed. Safety index was introduced as a measure of RF safety. It was shown that the resonance peak occurs approximately at half wavelength (approximately 21 cm inside a medium with a conductivity of 0.5 S/m and a relative permittivity of 80 which are representative for many tissues [29] ). For the bare wire case crucial safety index still exists

Based on Figure 2.3, it was concluded that only for wires having insulation of 30 percent of its radius and a length smaller than 10 cm, normal operating conditions are possible.

Curved wires were not investigated in this study. However intuitively it can be concluded that maximum current is induced on a wire when the electric field is coaxial with the wire. Curved wires possessing above mentioned properties (smaller than 10 cm, adequately insulated) will not heat more than a straight wire, given that the incident electric field is coaxial with the straight wire. In an MR scanner, due to coil characteristics, this direction is the z direction, which is the longitudinal direction of the cavity.

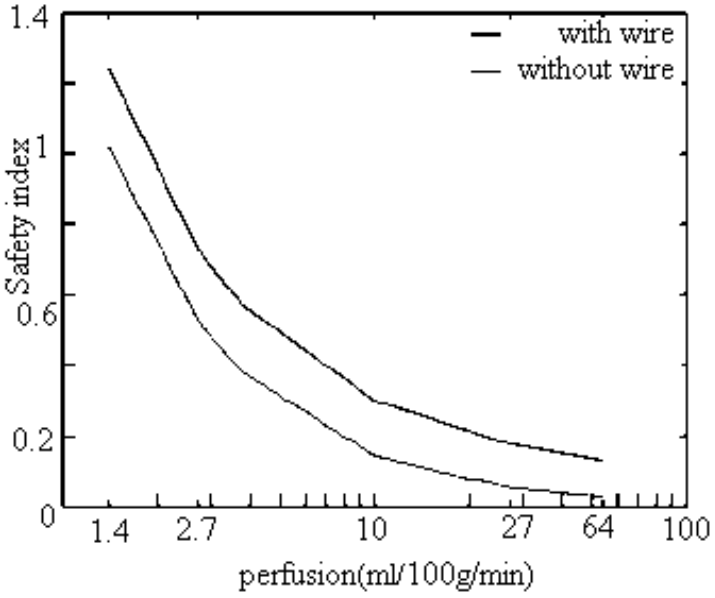


Figure 2.3: a 10-cm insulated wire (diameter = 0.5 mm, insulation thickness = 75 $\mu$m). Safety index for each wire is compared to the wire-free safety index [15] .

# Chapter 3

# Materials and Methods

Using the theory, presented in the previous chapter, several safety issues were investigated. First of all the validation of simulating perfusion in perfusionless phantom was performed via phantom and in-vivo experiments. Later, temperature increase due to a pacemaker was investigated and a safe pacemaker design is provided.

## 3.1 Simulating perfusion in a perfusionless phantom

Two antennas were used in phantom and in-vivo experiments: Loopless antenna and a thermal ablation probe. Loopless antenna is basically a coaxial cable with outer conductor peeled off at its distal end. It acts similarly to a dipole antenna and can be used in diagnosing atherosclerosis. A thermal ablation probe is used in heating tumors up to high temperatures till the tumor vanishes. It is composed of a plate, on which the animal is placed, and a wire that is to be inserted inside the tumor.

A series of phantom and in-vivo experiments (rabbit) were performed with these antennas (Figure 3.2). No matching circuitry was used. Power delivered to

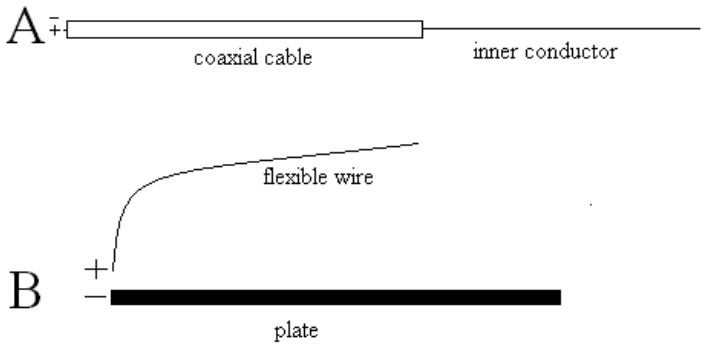


Figure 3.1: A) Loopless antenna: build by stripping the outer conductor of a coax, acts like a dipole and can be used in diagnosing atherosclerosis. B) Thermal ablation probe: build of a plate and a wire, it is used in thermal ablation of tumors.

the load is calculated using a network analyzer in experiments in which loopless coil was used, and using an oscilloscope in experiments in which thermal ablation probe was used.

Fiber optic probe is attached to the hot spots in all experiments. For a loopless coil, the hot spot is the distal end of the inner conductor, where outer conductor is peeled off. For the thermal ablation probe, the hot spot is the tip of the wire.

Animal preparation was performed as follows: Firstly, the rabbit was anesthetized with a mixture of 40 mg/kg Ketamine and 5 mg/kg xylazine through intramuscular and intravenous infusion. The doses were repeated each hour. In the experiment with thermal ablation probe, the rabbit was shaved to increase its conductivity. Then, an ultrasound gel was spread onto the parts of the skin that contacted the metal plate, to reduce contact resistance.

Temperature data from five tissues; muscle, fat, kidney, liver, brain were collected and compared with the data taken from phantom experiment. In the phantom experiment, the temperature at the instant of perfusion time constants for each tissue were compared with the steady state temperature rise that is found from the experiments.

In phantom experiments, gel is used to match electrical and thermal properties

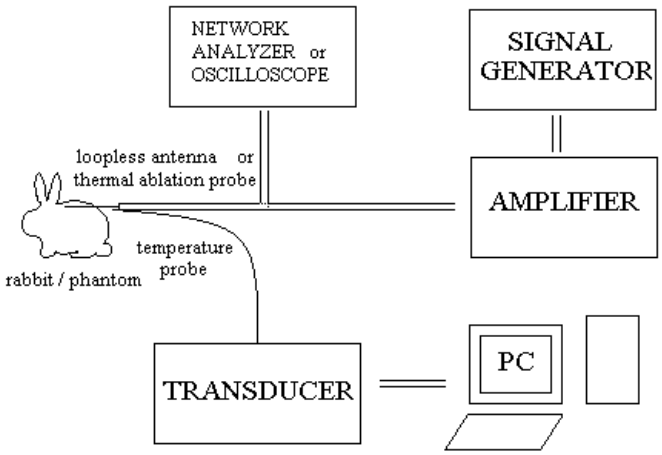


Figure 3.2: experiment setup: A loopless coil or a thermal ablation probe, fed via a signal generator and amplifier, is inserted into the tissue. A network analyzer or an oscilloscope is placed before the coil. An impedance measurement is performed to calculate power delivered to the subject.
Identical experiments are performed where the rabbit is replaced with a gel phantom. A fiber-optic probe is attached to the antennas for temperature measurement.

of tissues. Gel is a high water content material thus suitable for simulating tissue. In this study, jello was used as gel material. The electrical conductivity and permittivity were measured using a cylindrical capacitor. Both the theory and experiment for measuring the conductivity and permittivity are described in the appendix.

## 3.2 Electromagnetic Simulations

Solving the electromagnetic problem is a necessity when Green's function solution to the bioheat equation will be used to calculate the temperature increase caused by an implant. It is also needed when the expected temperature increase will be found with a phantom experiment as proposed before. It provides a comparison between the SAR values obtained using the simulation and the experiment.

The relationship between SAR and temperature increase in a phantom experiment comes from the bioheat equation. In the first few seconds of the experiment, since the spatial temperature distribution is relatively uniform, the laplacian term is omitted.

When the temperature distribution is uniform, as in the first few moments of data acquisition, the second derivative terms can be neglected since the spatial temperature gradient is very low. Also perfusion term is omitted since it does not exist, therefore we are left with:

$$\frac{1}{\alpha}\frac{d\Delta T(r,t)}{dt} = \frac{\rho_t}{k} SAR'(r,t) \tag{3.1}$$

Observing the temperature slope for the first few seconds and scaling it with appropriate constants it is possible to obtain SAR.

Throughout this thesis simulations were performed using an electromagnetic solver: FEKO (EMSS, Stellenbosch, South Africa). Medium parameters were assigned to have a relative permittivity of 80 and conductivity of 0.7 S/m for simulating heart tissue at 64 MHz (1.5 Tesla) [29].

Birdcage coil that is used in MRI is not modelled in the simulations. The pacemaker was excited with a plane wave having a frequency of 64 MHz, electric field pointing z-direction, based on the fact that the birdcage coil would create an electric field distribution that is approximately uniform around the pacemaker. Therefore a plane wave can serve for this purpose.

## 3.3 MR Experiment Methods

A GE Excite MR scanner was used. The following pulse sequence is used throughout the experiments. The amount of power transmitted is the crucial factor here. Other pulse sequences can also be used. One important parameter is the duty cycle of the pulse sequence which is deeply investigated in Appendix.

To be able to observe the temperature increase, a high power pulse sequence is recommended, therefore the transmit gain should be set to the maximum value. Entering a high weight to the patient will also force the scanner to transmit high power. In all the pulse sequences 350 kg (159 lbs) is entered as the weight of the patient. The predicted peak SAR was 8 W/kg. FSPGR pulse sequence with pulse repetition time: TR = 8 msec, echo time: TE = M-FUL, number of slices (NS) = 1, flip angle = 90 is used.

## 3.4 Safe wire

Heating of a half wavelength insulated wire was compared with the heating of a wire of the same length and an inductor as an RF choke, as seen in Figure 3.3.


Figure 3.3: An inductor is placed with short intervals to enhance RF safety. Shielding is used to ensure decoupling of the inductor with RF field

A half wavelength is the resonant length, i.e., it is the length at which most heating occurs. First, a simulation was performed with FEKO to observe whether the RF choke could block the induced current so that this wire acted as two separate wires of half the original length.

Gel phantom experiments were performed to verify the simulation results. The setup is shown in Figure 3.4 A GE Signa 1.5T MR scanner was used, with all the gradients shut off, and a body coil was used to irradiate the phantom. An AWG 24 wire with a 0.25 mm radius and 0.2 mm insulation thickness were used and situated at a constant radial position, but placed longitudinally in the phantom. The half wavelength for such a wire was found to be 22 cm using FEKO. The temperature was recorded using custom-built fiberoptic temperature

probes (FISO Technologies, Ste. Foy, Quebec, Canada).

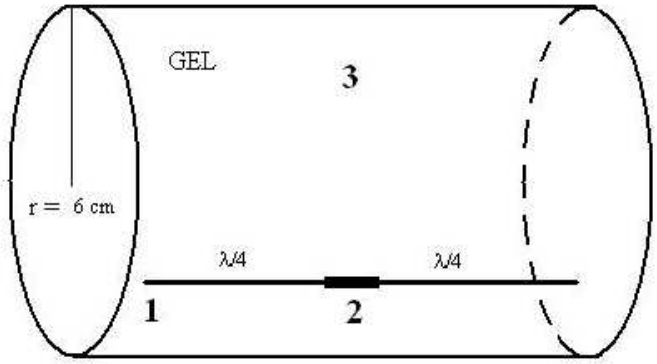


Figure 3.4: Safe wire experiment setup: Regular and safe wires were inserted into cylindrical gel phantoms and MR scanned. During the scan, temperature was recorded via fiber optic temperature sensors. 1 and 2 represent temperature probes located at the tip and the middle of the wire. 3 is the reference probe. All probes are equidistant from the origin.

## 3.5 Safe implantable device

A safe wire design implementation is demonstrated. Longer safe wires can be used in metallic implants for communication between the signal generator and the organ, if RF chokes are placed in short intervals. Patients using such implants can be scanned with no additional RF heating. Refer to Figure 3.5 for an illustration of the safe DBS as an example.

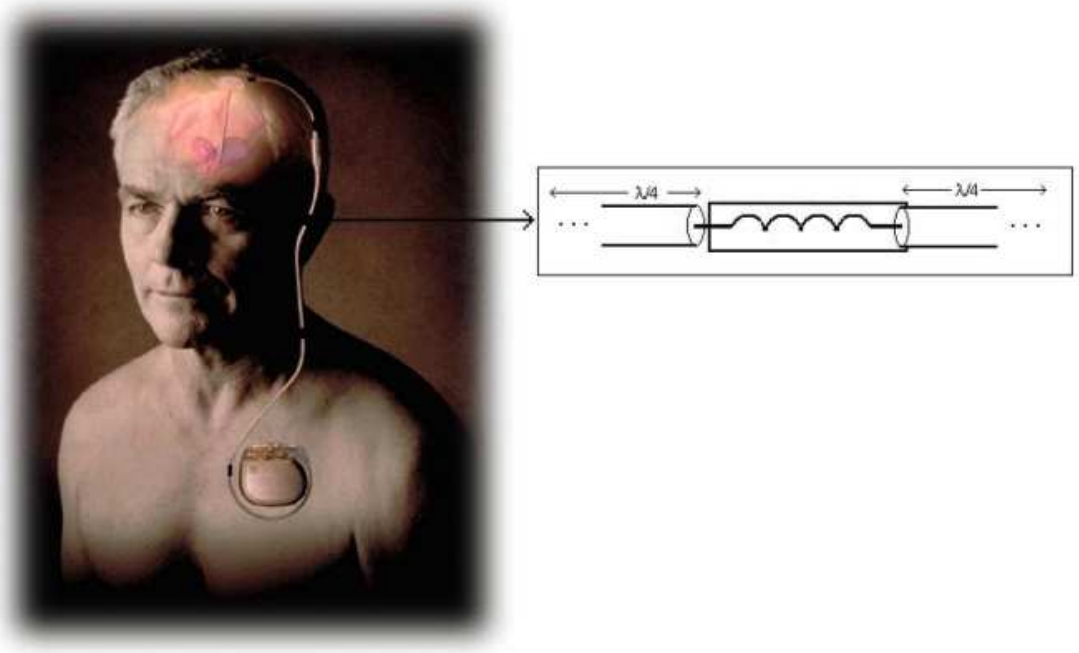


Figure 3.5: Illustration of a safe DBS. The picture is modified from www.henryfordhealth.org

Experiments and simulations were performed on a pacemaker. A pacemaker was modelled in FEKO as shown in Figure 3.6. The curvature of the lead depends on the shape of the main vein, the superior venacava. The figure shows a typical placement in human body.

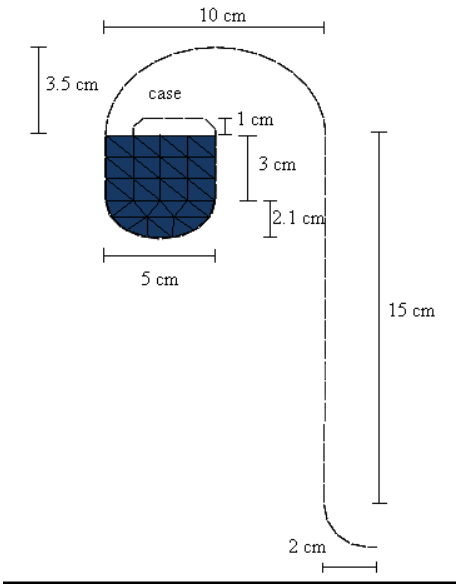


Figure 3.6: FEKO model for a pacemaker: The model was formed based on heat maximization and geometry. The curvature of the lead was formed considering the vein it is located in. Lead length and lead-generator connection capacitance was adjusted so that maximum heating occurred at the tip

*Pacemaker model*

The case of the pacemaker is 0.8 mm thick. On y-z plane, the case is modelled by the combination of a 5x3 cm rectangle (on top) with a half ellipse (bottom) having an elliptic ratio of 0.7. Elliptic ratio is the ratio of the horizontal dimension of an ellipse to its vertical dimension (for instance, it is obviously 1 for a circle).

The wire is connected to a spot that is 1.25 cm from the upper-left corner of the case, it goes up 1 cm, turns right until it is on the same level with the upper-right corner of the case. Then the lead takes one tour around the case. It is directly connected to the case since this is the worst case situation in terms of heating. After one tour around the case, another half ellipse with 0.7 elliptic ratio is travelled. Now we are 5 cm away from the right top corner of the case. Then the wire goes 15 cm downward and makes a quarter circle of radius 2 cm.

The wire diameter is 0.8 mm and the coating thickness is 0.35 mm. Relative insulation permittivity is 2.3. This is the relative permittivity of polyolefin, a commonly available heat shrink material. 5 mm at the tip of the lead is left uninsulated. Total length of the lead is 50 cm.

The pacemaker, modelled in the simulation, was built. The case contained no circuitry, since it is not needed while investigating the heating. Electromagnetically the problem is the same whether the circuitry is included or not. An identical pacemaker was built, but this time RF chokes were placed in between short intervals. Both pacemakers can be seen in Figure 3.7.

These pacemakers were placed in two cylindrical gel-phantom and placed inside MR scanners. Fiber optic temperature probes were placed at the tip of the lead, which is the hot spot, most heating location, according to simulations, and at a distal spot as a reference. Both of these spots were equidistant from the ori8gin of the phantom for comparison (Figure 3.8). The distant spot serves as a reference.

Figure 3.7: Home-made pacemakers. Left: The pacemaker that was modelled in the simulation. Right: Safe pacemaker in which RF chokes are placed with short intervals.

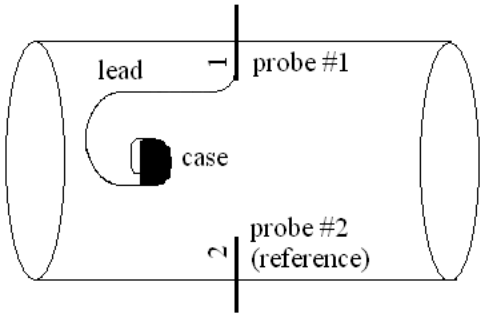


Figure 3.8: Experimental setup: probe 1 is placed at the tip of the pacemaker lead and Probe 2, the reference probe, is placed at a far point, equidistant to the origin with Probe 1.

## 3.6 Variational designs

Due to certain reasons such as spatial restrictions, isolation, inductance value, the default design may be undesirable and in such cases variational designs may be used. For instance shielding may be removed due to spatial restrictions (Figure 3.9 upper) however in this configuration there is the risk of magnetic coupling. Shielding is preferable to overcome this problem (Figure 3.9 - middle). Also a double sided shielding can provide an improvement in terms of decoupling the magnetic field (Figure 3.9 - bottom).

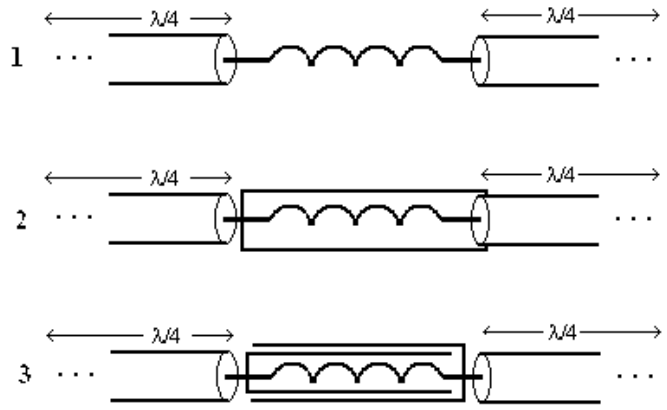


Figure 3.9: Variations on the design: shielding. 1) no shielding: may be used when there is space restriction. 2) Shielding to overcome coupling with RF. 3) double shielding: for improvement in decoupling

The usage of a core inside the inductor will provide higher inductance for a given resistance (Figure 3.10), in other words a better trap can be achieved if a cored inductor is used. Ferromagnetic cores should not be used to prevent any attraction by the static magnetic field. Also ferromagnetic cores would saturate under static magnetic field and thus act as a non magnetic material. Paramagnetic materials can be used as a core.

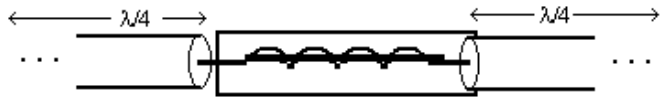


Figure 3.10: Variations on the design: cored inductor as an RF choke provides higher inductance. A better trap can be achieved this way.

Also, toroids can be used in the design, this way there may be no need for shielding, since the magnetic field is trapped inside the core (Figure 3.11).

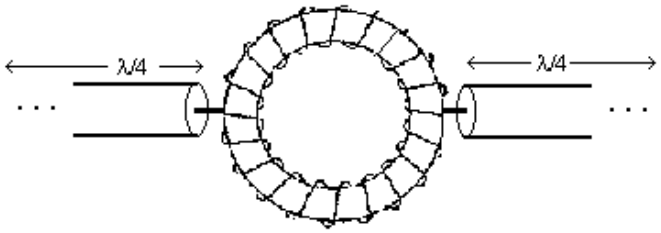


Figure 3.11: Variations on the design:toroid as an RF choke where shielding is not required since magnetic field is trapped inside the core.

Up to now, all designs were shown on a single wire model, however for a typical metallic implant there are several wires inside the lead. For instance in a DBS lead there are 4 wires inside the lead. To ensure safety the traps can be implemented by fastening all wires as an inductor (Figure 3.12). In other designs, traps can be placed in all the wires or a single toroid can be used for all wires.


Figure 3.12: Variations on the design: four wire safe lead is a practical way of making four traps in one.

RF traps can be formed using capacitors as well. All wires can be connected to the shield via capacitors (Figure 3.13). In this case, at high frequencies all wires are grounded and therefore no signal is being transmitted to the organ. Charges will be accumulated at the sharp edges of the shield. Insulating the shield as well as the other parts of the lead will provide further safety.

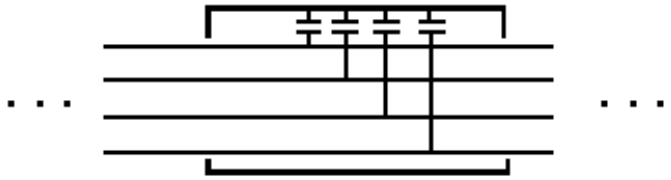

Figure 3.13: Variations on the design: implementation with capacitors

Throughout this chapter, the theory of predicting in vivo temperature increase from phantom experiments was given. Using this information, the next chapter aims to investigate temperature increase caused by regular and safe pacemakers.

# Chapter 4

# Results

## 4.1 Simulating perfusion in a perfusionless phantom

The data shown in the following figures (Figure 4.1, 4.2, 4.3) were obtained in a set of experiments. Heating of 5 different tissues, muscle, fat, kidney, liver and brain were investigated on rabbits. Loopless antenna was used in the muscle. Thermal ablation probe was used in other tissues since it was more flexible and easy to insert.

Temperature profile versus time profile for Temperature curve for the phantom experiment with loopless antenna is plotted in Figure 4.1, in-vivo experiment (muscle tissue) with the same antenna is plotted in Figure 4.2. Temperature curve for phantom experiment with thermal ablation probe, and in vivo experiments (fat, liver, kidney, brain) all plotted in Figure 4.3. The power levels are normalized with respect to the power delivered in phantom experiments for direct comparison.

Time constant determines how local the heating is in the phantom experiment. In a loopless antenna, the SAR surrounding the antenna resembles a line source [25] whereas a thermal ablation probe acts more like a point source. That is why the temperature increase is more slow, time constant is longer, in loopless antenna

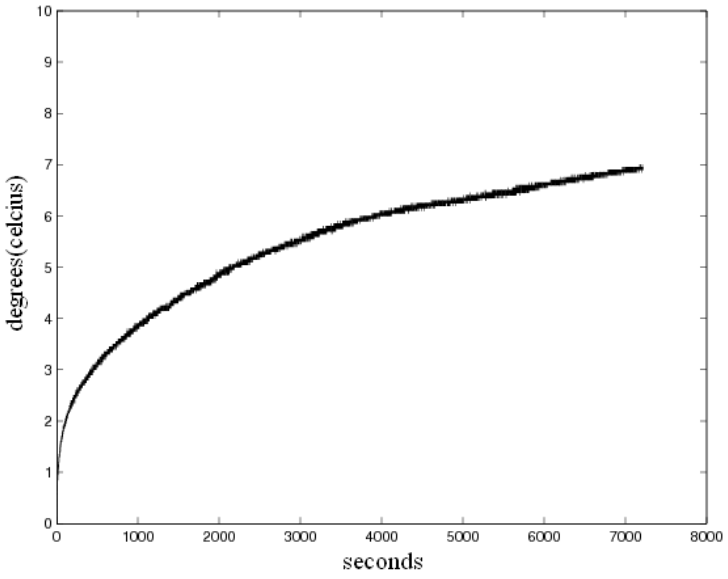


Figure 4.1: Heating curve for phantom experiment with loopless antenna

when compared to thermal ablation probe (Refer to Figure 4.3 for heating curve of phantom experiment with thermal ablation probe).

Experiment with the loopless antenna was conducted (Figure 4.2) on the hip of a rabbit, composed of muscle tissue (resting muscle). The heating curve obtained for this tissue, and for all other tissues as well, are not as smooth as the ones that are obtained in a phantom experiment due to several possible reasons. Eventhough the rabbit is under anesthesia, minor involuntary movement is frequently observed. Especially near the abdominal region, as temperature increases, the breathing rate experiences rapid changes which results in tiny spikes on the heating data. Also the response of the body to this temperature increase is crucial. It is known that perfusion increases when body temperature increases. This may even cause a drop in temperature during the experiment.

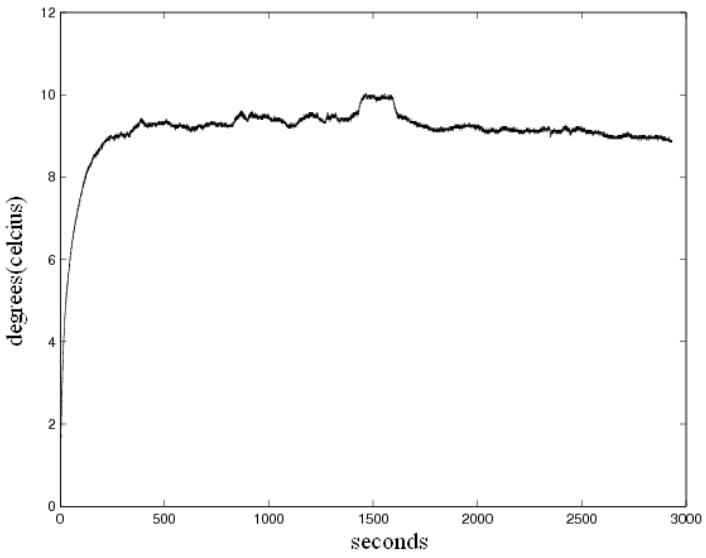


Figure 4.2: Heating curve for muscle tissue; deviation from the steady state temperature is observed around 1500 seconds due to minor movement of the rabbit.

The data are also shown in Table 4.1.

| Tissue | temperature increase | time constant | estimate | error |
|---|---|---|---|---|
| muscle | 9 | 2220 | 5.05 | 44 |
| fat | 2.5 | 1128-1620 | 3.2-3.3 | 21.8-24 |
| kidney | 0.62 | 11.4-14 | 0.8-0.9 | 22.8-31 |
| liver | 0.75 | 48-102 | 1.75-2.2 | 57-66 |
| brain | 0.84 | 108 | 2.1-2.2 | 60-61.8 |

Table 4.1: All the data above are normalized to the same level of delivered power. Data obtained from experiments that are performed on tissues are compared with phantom experiment estimates.

In conclusion, prediction error up to 66 percent was observed. The main reason is the mismatch between thermal and electrical properties of phantom and tissues. More accurate results may be obtained if different gels were used for simulating different tissues. Electrical properties of the gel and all the tissues (except fat) matches. However no measurement was performed regarding thermal properties, which differs significantly from tissue to tissue. Considering all this a maximum error of 66 percent is reasonable. Introducing a safety factor of 2 and reporting double the predicted temperature would ensure that in-vivo

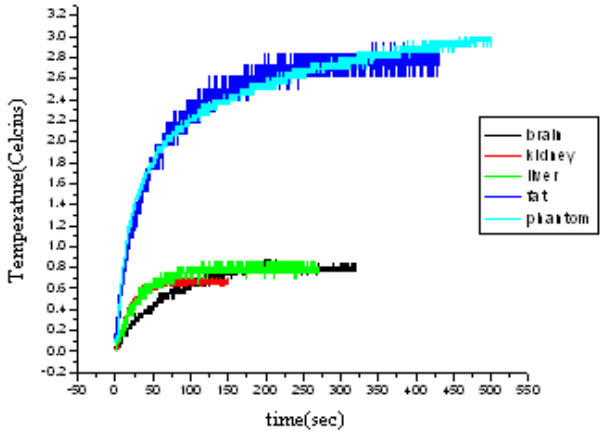


Figure 4.3: Experiment with thermal ablation probe. Heating curve for all tissues and phantom.

temperature increase is bounded with the reported value, which would ensure safe scans.

Eventhough no MR scanner was used in the experiments, the theory is applicable in any environment with an RF transmitter. This information can be used for setting safety limits in MRI, carefully considering the amount of prediction error that can exist due to mismatch of phantom properties.

## 4.2 Simulations of safe wire

Simulation results are depicted in Figure 4.4. Figure 4.4 A shows the induced current on the half wavelength wire and the safe wire that is also half wavelength with an RF choke in the middle. Figure 4.4 B shows the SAR distribution on the surface of the half wavelength wire and safe wire. From these simulations, it is obvious that the safe wire is able to separate a resonant length wire into two quarter wavelength wires, ensuring safety. Temperature profiles of experiments with regular and safe resonant length wires are shown in Figure 4.5 . Note that the temperature increases at the tip of the wires drop with the insertion of the inductor. SAR gain, i.e., the amplification in the SAR due to the presence of the wire, can be calculated by taking the ratio of the temperature increase of

the probe located at the tip of the wire to the reference probe. Experimentally, the SAR gain was observed to be approximately 21 and 1.2 for regular and safe wire, and, from the simulations, these values were found to be 26 and 1.45. These results lay within the error margin of the experiments. Since the SAR gain of the safe wire was found to be around 1, without solving the bioheat equation, intuitively it can be concluded that the temperature increase will be same as for the case where no wire exists. For typical perfusion rates , the safety index, temperature increase per unit of applied SAR of 0.02 $^oC$/W/kg in the heart, is well below FDA limits

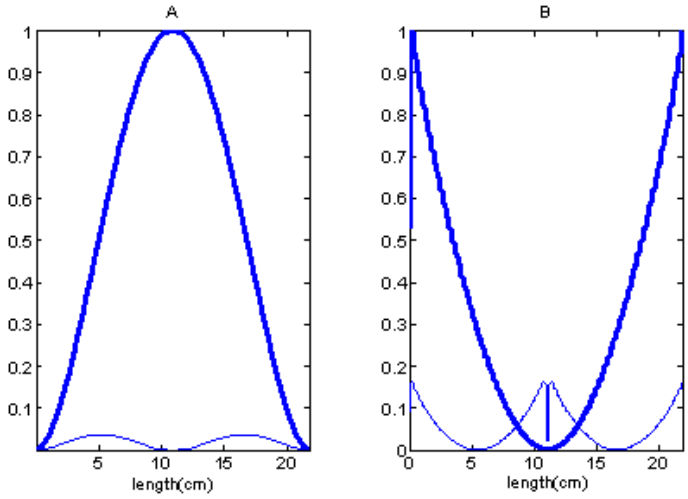


Figure 4.4: (A) Induced current on regular wire (thick) and on safe wire (thin). (B) SAR tangent to regular wire (thick) and safe wire (thin). The values are normalized with respect to maximum values of regular wire curves.

After the test of a safe wire, a safe pacemaker was built with the same manner, RF chokes placed with small intervals. The temperature curves for a regular pacemaker and safe pacemaker are as follows:

5 W/kg of peak input SAR caused a 0.5 degrees Celsius increase in the reference spot, 1.5 degrees Celsius in the safe pacemaker and 11 degrees Celsius in the regular one. Based on the fact that the perfusion time constant for heart tissue is 1.2 minutes, the expected steady state in-vivo temperature increase is 5.4 degrees for the regular pacemakers whereas it is a 0.45 degrees Celsius in the safe one.

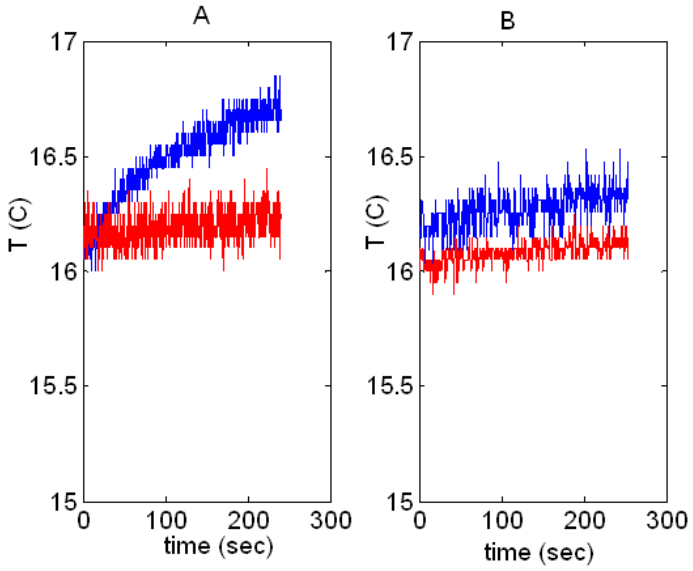


Figure 4.5: (A) Regular wire(B) safe wire. Eventhough small amount of power is delivered by the scanner, the difference between the initial slopes of temperature curves proves the improvement in safety.

In-vivo temperature increase was also calculated with convolving Green's function to the bioheat equation with the SAR distribution around the tip of the pacemaker. Cylindrical symmetry was assumed around the tip. Spatial resolution was doubled until the result obtained with two consecutive resolutions differed (on the absolute average) less than 2 percent. The temperature increases found with convolution were 7.1 degrees Celsius for the regular pacemaker and 0.75 degrees Celsius for the safe pacemaker respectively.

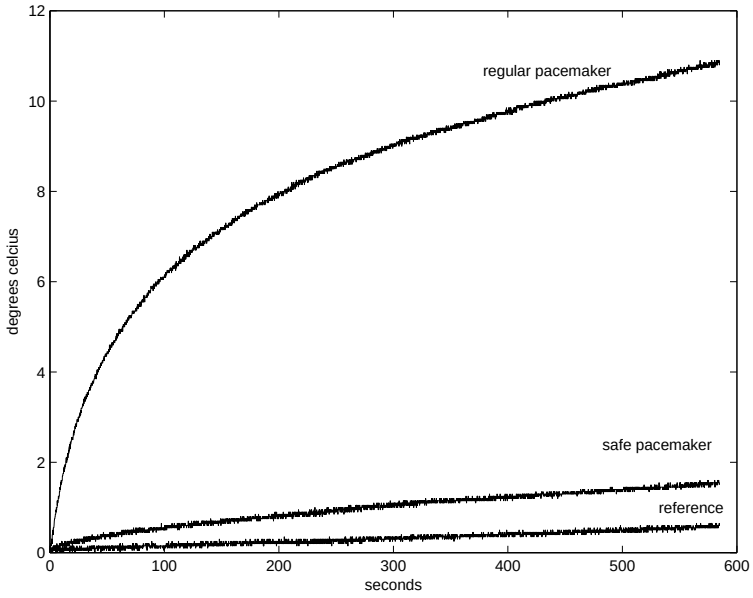


Figure 4.6: Heating curves at the tip of a regular pacemaker, pacemaker with RF chokes placed with short intervals, and the reference probe which is located equidistant from the tip to the surface of the phantom, placed at a distant position

# Chapter 5

# Conclusion and Future Work

A method was demonstrated for performing Green's function of the bioheat equation weighted SAR averaging. This was used to simulate physiological parameters for predicting steady state temperature changes in tissues, in a phantom where these parameters are absent. This RF safety measurement approach is a straightforward way to examine RF heating when invasive or implanted metallic devices are present during MRI.

Using the demonstrated method, a safe wire design implementation is demonstrated. Longer safe wires can be used in metallic implants for communication between the signal generator and the organ, if RF chokes are placed with short intervals. A pacemaker with such a lead was built and tested. Patients using such pacemakers can be scanned with no additional RF heating. Introducing RF chokes on the wire will lead into some degradation of the transmitted signal. Since almost no loss is observed on the cables, the same power will be transmitted to the organ. Rather than the shape of the transmitted pulse, it is the power of the pulse that creates an action potential on cell membranes; thus, this degradation can be tolerated. If a high inductance value is used, the RF choke becomes a better trap for the current, whereas signal degradation increases. This trade-off should be carefully investigated.

RF chokes should not be a handicap in terms of the flexibility of the lead.

In this thesis, three non-magnetic chip inductors were serially connected on a tiny printed circuit board to achieve 1 kilo ohms impedance and adequate quality factor. In this sense, achieving this with a single inductor is better.

Safe implantable device design is advantageous over other possible safe designs due to previously listed reasons. Furthermore, it is the most easy one to implement. Experiments and simulation results show that, safe scans can be performed on patients with implantable devices implemented using this design. The proposed analysis is valid for any implantable device with leads and it can also be used in guidewires and catheters in the same manner.

Future work involves testing the safe pacemaker on animals. After a set of experiments these devices will be closer to being reality, a part in our lives.

# Bibliography


[1] http://www.gemedicalsystems.com

[2] Nair P, Roguin A. Magnetic Resonance Imaging in patients with ICDs and Pacemakers. Indian Pacing and Electrophysiology Journal (ISSN 0972-6292), 5(3): 197-209 (2005).

[3] Shellock F G. Magnetic Resonance Safety update 2002: Implants and Devices. JMRI 2002:16:485-496

[4] Achenbach S, Moshage W, Diem B, Bieberle T, Schibgilla V, Bachmann K. Effects of magnetic resonance imaging on cardiac pacemakers and electrodes. Am Heart J 1997;134:467-473.

[5] Sommer T, Hahlhaus C, Lauck G, et al. MR imaging and cardiac pacemakers: in vitro evaluation and in vivo studies in 51 patients at 0.5 T. Radiology 2000;215:869-879.

[6] http://www.ahc.umn.edu

[7] Hofman MB, de Cock CC, van der Linden JC, et al. Transesophageal cardiac pacing during magnetic resonance imaging: feasibility and safety considerations. Magn Reson Med 1996;35:413-422.

[8] Smith CD, Kildishev AV, Nyenhuis JA, Foster KS, Bourland JD. Interactions of MRI magnetic fields with elongated medical implants. J Applied Physics 2000;87:6188-6190. 8.

[9] Smith CD, Nyenhuis JA, Kildishev AV. Health effects of induced electrical currents: implications for implants. In: Shellock FG, editor. Magnetic resonance: health effects and safety. Boca Raton, FL:

[10] Konings MK, Bartels LW, Smits HJ, Bakker CJ. Heating around intravascular guidewires by resonating RF waves. J Magn Reson Imaging 2000;12:79-85.

[11] Nitz WR, Oppelt A, Renz W, Manke C, Lenhart M, Link J. On the heating of linear conductive structures as guide wires and catheters in interventional MRI. J Magn Reson Imaging 2001;13:105-114.

[12] Kanal E, Shellock FG. Burns associated with clinical MR examinations [Letter]. Radiology 1990;175:585.

[13] Rezai AR, Finelli D, Nyenhuis JA, et al. Neurostimulator for deep brain stimulation: ex vivo evaluation of MRI-related heating at 1.5-Tesla. J Magn Reson Imaging 2002:15:241-250.

[14] FREEHAND System. Package insert. NeuroControl Corporation, Cleveland, OH

[15] Yeung CJ, Susil RC, Atalar E. RF safety of wires in intervetional MRI: Using a safety index. Magn Reson Med 2002; 47:187-193.

[16] Ferhanoglu O, Tasci O.T, El-Sharkawy A, Altintas A, Atalar E. Investigating RF Heating of pacemakers in MRI using a safety index, Proc. International Society of Magnetic Resonance in Medicine, 12th Scientific Meeting, Kyoto, 2004

[17] Ferhanoglu O, El-Sharkawy A, Atalar E. RF Heating at the tip of pacemaker leads, Proc. European Society of Magnetic Resonance in Medicine and Biology, 21st Scientific Meeting, Copenhagen, 2004

[18] 17. Atalar E, Enhanced Safety Coaxial Cables, United States Patent No: 6,284,971

[19] 18. Susil RC et al., Multifunctional Interventional Devices for MRI: A Combined Electrophysiology/MRI Catheter, MRM 47:594-600 (2002).

[20] Ladd ME et. al., Reduction of Resonant RF Heating in Intravascular Catheters Using Coaxial Chokes, MRM 43:615-619 (2000).

[21] Thompson et al, Implantable medical device incorporating integrated circuit notch filters, US Patent no: 6,539,253, 2003

[22] Nappholz et. al, Rate-responsive pacemaker with minute volume determination and EMI protection, US Patent no: 5,817,136, 1998

[23] Tsitlik J.E et. al., ECG Amplifier and Cardiac Pacemaker for use during Magnetic Resonance Imaging, US Patent no: 5,217,010, 1993.

[24] Greatbatch W, Miller V, Shellock FG. Magnetic resonance safety testing of a newly-developed, fiber-optic cardiac pacing lead. J Magn Reson Imaging 2002; 16:97-103.

[25] Yeung CJ, Atalar E. A Green's function approach to local RF heating in interventional MRI. Med Phys 2001; 28:826-832.

[26] U.S. Department of Health and Human Services, Food and Drug Administration, Center for Devices and Radiological Health, Guidance for the submission of premarket notifications for magnetic resonance diagnostic devices US DHHS FDA, Rockville, MD, 1998.

[27] H.H.Pennes,Analysis of tissue and arterial temperatures in the resting human forearm, J.Appl.Physiol.1,931221948

[28] D.K.Cheng, Field and Wave Electromagnetics, Addison-Wesley Publishing Company, 1992

[29] http://www.fcc.gov/fcc-bin/dielec.sh

[30] http://www.brooks.af.mil/AFRL/HED/hedr/reports/dielectric/Report/Report.html

[31] Yeung Christopher, "Safety issues in Magnetic Resonance Imaging", Dissertation for the Degree of Doctor of Philosophy, Johns Hopkins University, School of Medicine, 2003.

[32] http://www.bbraunusa.com/stimuplex/pens1.html

[33] http://www.bbraunusua.com/stimuplex/pens1.html

# Appendix A

# Measuring conductivity and permittivity of a given material

A cylindrical capacitor was used for this purpose. Due to the conductive material inside, it was modelled as a lossy transmission line. All the formulas used in the following theory is taken from [28], 9th chapter:Theory and Application of Transmission Lines.

The characteristic impedance of a lossy T.L (Transmission line) is given by

$$Z_0 = \sqrt{\frac{R + jwL}{G + jwC}} \tag{A.1}$$

assuming that the transmission line is made using a good conductor (copper for instance) R is much smaller than jwL, the equation becomes:

$$Z_0 = \sqrt{\frac{jwL}{G + jwC}} \tag{A.2}$$

The input impedance is given by:

$$Z_{in} = Z_O . \frac{Z_L + Z_O \tanh(\gamma l)}{Z_O + Z_L \tanh(\gamma l)} \tag{A.3}$$

since the T.L is open, input impedance can be further simplified to:

$$Z_{in} = \frac{Z_O}{\tanh(\gamma l)} \tag{A.4}$$

where the complex wavenumber is given by

$$\gamma = jw\sqrt{\mu\varepsilon}(1 + \frac{\sigma}{jw\varepsilon})^{1/2} \tag{A.5}$$

$Z_{in}$ is obtained from the measurement taken by the network analyzer in r - jx form.

To obtain $Z_O$, the following formulas should be used:

$$L = \frac{\mu}{2\pi} \ln \frac{b}{a}(H/m) \tag{A.6}$$

where a and b are inner and outer diameter of the cylindrical capacitor respectively.

$$G = \frac{2\pi\sigma}{\ln(b/a)}(S/m) \tag{A.7}$$

$$C = \frac{2\pi\varepsilon}{\ln(b/a)}(F/m) \tag{A.8}$$

Then, make an initial guess for the conductivity, substitute it into the complex wavenumber equation and plot both $\frac{Z_O}{\tanh(\gamma l)}$ and $Z_{in}$ with respect to relative permittivity (both real and imaginary parts, therefore we have two plots). since they have to be the same according to eq. A.4. Modify the conductivity until the intersection in both plots have the same relative permittivity value. relative epsilon and conductivity values that provide intersection in both graphs are the ones we are looking for.

Although not necessary, the following lines will provide an ease in making an initial conductivity guess. Making such a guess requires conductivity data to be taken at low frequencies. For instance if we are seeking for 64 MHz (1.5 Tesla) data, at least one octave below (6.4 MHz) should be used. At such low frequencies, one can assume that R is much smaller than $jwL$ and $jwC$ is much smaller than G. Under these assumptions $Z_O$ and $\gamma$ become :

$$Z_O = \sqrt{\frac{jwL}{G}} \tag{A.9}$$

$$\gamma = jw\sqrt{\frac{\mu\sigma}{jw}} \tag{A.10}$$

at low frequencies permittivity does not take part in these equations. To find the conductivity plot both plot both $\frac{Z_O}{\tanh(\gamma l)}$ and $Z_{in}$ with respect to conductivity (both real and imaginary parts, two plots in total). If x is much smaller than r in the network analyzer measurement (which is the case for low frequencies) both intersections should be the same.

Use this conductivity value as an initial guess to find the conductivity value at high frequency. According to U.S Air Force Research Lab (AFRL) findings conductivity values increase by an average amount of (average of all tissues) 20 percent [29], therefore this initial guess will be good enough.

Using the proposed method, the conductivity of KCl solution was measured and compared with the data obtained by AFRL. [33]. The results were in perfect agreement.

In safety experiments gel phantoms are used since they do not experience convection likewise tissues. Convection is observed when liquid phantoms are used. Gel phantoms can even be made with materials that can be found in the supermarket (jello, starch). The water and salt content added to these materials may be adjusted to simulate various tissues.

# Appendix B

# Conductivity and Permittivity of Tissues at 64 MHz

The table below is taken from AFRL's web site [29].

| Tissue | Relative Permittivity | Conductivity (S/m) |
|---|---|---|
| Bladder | 24 | 0.28 |
| Blood | 86 | 1.20 |
| Bone (Cancellous) | 30 | 0.16 |
| Bone (Cortical) | 16 | 0.06 |
| Bone marrow (Infiltrated) | 16 | 0.15 |
| Bone marrow (Not Infiltrated) | 7 | 0.02 |
| Breast Fat | 6 | 0.03 |
| Cartilage | 62 | 0.45 |
| Cerebellum | 116 | 0.71 |
| Cerebrospinal Fluid | 97 | 2.06 |
| Colon (Large Intestine) | 94 | 0.63 |
| Cornea | 87 | 1.00 |
| Dura | 73 | 0.70 |
| Eye Tissue(Sclera) | 75 | 0.88 |
| Fat | 7 | 0.04 |
| Fat(Mean) | 13 | 0.07 |

Table B.1: Permittivity and conductivity of tissues at 64 MHz

| Tissue | Relative Permittivity | Conductivity (S/m) |
|---|---|---|
| Gall Bladder | 87 | 0.96 |
| Gall Bladder Bile | 105 | 1.48 |
| Grey Matter | 97 | 0.51 |
| Heart | 106 | 0.67 |
| Kidney | 118 | 0.74 |
| Lens Cortex | 60 | 0.58 |
| Lens Nucleus | 50 | 0.28 |
| Liver | 80 | 0.44 |
| Lung (Inflated) | 37 | 0.28 |
| Lung (Deflated) | 75 | 0.53 |
| Muscle (Parallel Fiber) | 71 | 0.73 |
| Muscle (Transverse Fiber) | 72 | 0.68 |
| Nerve (Spinal chord) | 55 | 0.31 |
| Ovary | 106 | 0.68 |
| Skin (Dry) | 92 | 0.43 |
| Skin (Wet) | 76 | 0.48 |
| Small Intestine | 118 | 1.59 |
| Spleen | 110 | 0.74 |
| Stomach Esop Duodenum | 85 | 0.87 |
| Tendon | 59 | 0.47 |
| Testis Prostate | 84 | 0.88 |
| Thyroid Thymus | 73 | 0.77 |
| Tongue | 75 | 0.65 |
| Trachea | 58 | 0.52 |
| Uterus | 92 | 0.91 |
| Vitreous Humour | 69 | 1.50 |
| White Matter | 67 | 0.29 |

Table B.2: Permittivity and conductivity of tissues at 64 MHz: continued

# Appendix C

# Effect of Duty Cycle on Heating, in MRI

Various pulse sequences have different duty cycles, in MRI. A high duty cycle leads into a steady state temperature increase. On the other hand if a pulse sequence with a low duty cycle is used, temperature deviates in between two values, upper and lower thresholds. This section aims to investigate this effect.

In order to do so, the Bioheat equation (eq 2.2) is going to be discretized using the finite difference time domain method. derivative with respect to time, on the left hand side of the equation is handled as follows:

$$\frac{dT}{dt} = \frac{T_{t+1} - T_t}{\Delta t} \tag{C.1}$$

where $\Delta t$ is the time resolution, and subscripts t's indicate discrete time instants. Laplacian term in spherical coordinates is given as:

$$\nabla^2 T = \frac{1}{R^2}\frac{\delta}{\delta R}(R^2\frac{\delta T}{\delta R}) \tag{C.2}$$

Taking the derivative of the multiplicative term, the laplacian becomes:

$$\nabla^2 T = \frac{1}{R^2}(2R\frac{\delta T}{\delta R} + R^2\frac{\delta^2 T}{\delta R^2}) \tag{C.3}$$

Second derivative of temperature with respect to R is discretized as follows:

$$\frac{\delta^2 T}{\delta R^2} = \frac{(\frac{T_{R+1}-T_R}{\Delta R}) - (\frac{T_R - T_{R-1}}{\Delta R})}{\Delta R} \tag{C.4}$$

where $\Delta R$ is the spatial resolution, and subscripts R's indicate discrete space locations in spherical coordinates. With further simplification:

$$\frac{\delta^2 T}{\delta R^2} = \frac{T_{R+1} + T_{R-1} - 2T_R}{\Delta R^2} \tag{C.5}$$

Now we have everything we need to write discretized Bioheat equation:

$$\frac{1}{\alpha}\frac{T_{t+1,R} - T_{t,R}}{\Delta t} = \frac{2}{R}(\frac{T_{t,R} - T_{t,R-1}}{\Delta R}) + \frac{T_{t,R+1} + T_{t,R-1} - 2T_{t,R}}{\Delta R^2} - v^2 T_{t,R} + \frac{\delta_t}{k} SAR_{t,R} \tag{C.6}$$

If time instant = t terms are gathered on the left side, a ready to program form of the Bioheat equation is formed.

$T_{t+1,R} = \alpha \Delta t(T_{t,R}(\frac{1}{\alpha \Delta t} + \frac{2}{R\Delta R} - \frac{2}{\Delta R^2} - v^2) + T_{t,R-1}(-\frac{2}{R\Delta R} + \frac{1}{\Delta R^2}) +$
$T_{t,R+1}(\frac{1}{\Delta R^2} + \frac{\delta_t}{k} SAR_{t,R})$

A for loop with time variable is needed to obtain temperature curve with respect to time. Also SAR with respect to space should be entered before the loop, considering the duty cycle it should be turned on and of inside the time loop.

A spherical phantom was excited through its center as shown in the figure. First, temperature increase in the center of the spheres was investigated. The mass of the excited region was varied (R0 was varied) and time constant, time instance where 63 percent of the steady state temperature is reached, was observed for exercising muscle cell.

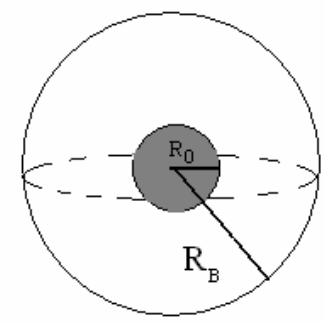


Figure C.1: Spherical phantom of radius $R_B$, is excited through a smaller sphere (gray region) with radius $R_0$.

The steepest temperature increase is observed when the excited region has the smallest volume. In this case, conduction is the leading factor in heat transfer (laplacian term in bioheat equation). As the size of the excited region increases perfusion becomes the leading term and the time constant approaches perfusion time constant. The following table summarizes the data.

| $R_O$ | Weight of the excited region (grams) | Time constant (sec) |
|---|---|---|
| 1 mm | $4\text{x}10^{-3}$ | 5 |
| 2 mm | $34\text{x}10^{-3}$ | 17 |
| 3 mm | $113\text{x}10^{-3}$ | 31 |
| 4 mm | $268\text{x}10^{-3}$ | 46 |
| 5 mm | $524\text{x}10^{-3}$ | 60 |
| 6 mm | $905\text{x}10^{-3}$ | 73 |
| 7 mm | 1.4 | 86 |
| 8 mm | 2.4 | 99 |
| 9 mm | 3.1 | 110 |
| 10 mm | 4.2 | 121 |
| 20 mm | 33.5 | 188 |
| 30 mm | 113.5 | 206 |

Table C.1: time constants with respect to excitation mass in exercising muscle cell, refer to figure C.2, perfusion time constant for exercising muscle cell is 222 seconds.

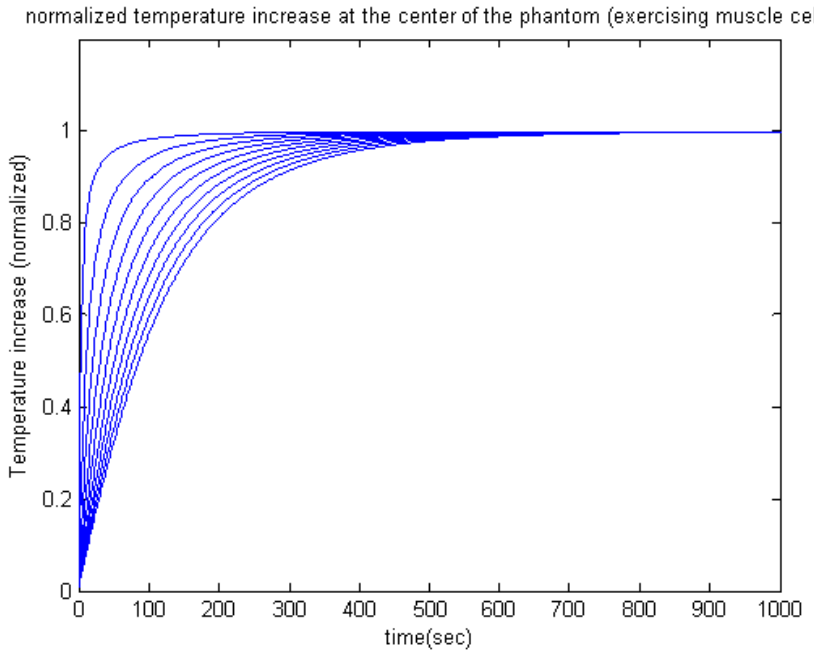


Figure C.2: Among 12 curves, the one with the most rapid rise is excited with smallest volume and vice versa.

Up to this point the power was applied continuously in all time instances. The following table indicates what happens to the steady state temperature when the power is applied as periodic pulses with different duty cycles. In all cases, applied power is constant. Steady state temperature increase is normalized with respect to the case where duty cycle is The simulation is performed for resting muscle cell tissue, radius of the excited volume being 5 cm. The radius of the phantom is 10 cm.

| Duty cycle(percent) | TR = 500 sec | TR = 1000 sec | TR = 2000 sec |
|---|---|---|---|
| 100 | 1 | 1 | 1 |
| 50 | 1.07 | 1.14 | 1.27 |
| 10 | 1.13 | 1.26 | 1.55 |
| 1 | 1.14 | 1.29 | 1.63 |
| 0.1 | 1.14 | 1.30 | 1.63 |
| 0.05 | 1.14 | 1.30 | 1.63 |

Table C.2: When duty cycle is below 100 percent, temperature deviates in between a lower threshold and an upper threshold. The upper threshold is usually greater than the steady state temperature for continuous input power (Duty Cycle = 100) When repetition time (TR) increases, this effect is more stressed .

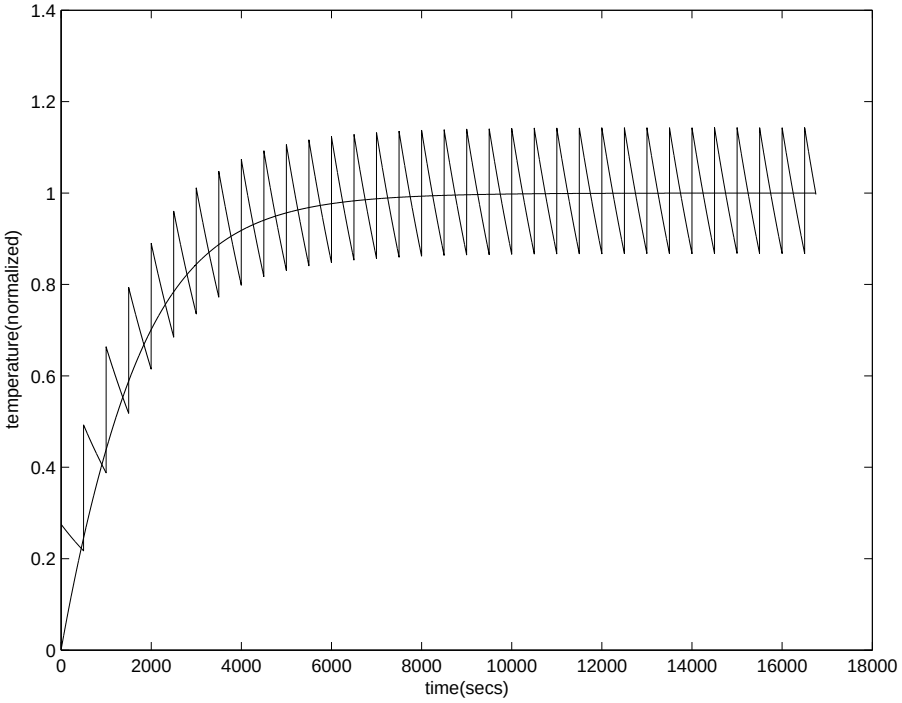


Figure C.3: The smooth line belongs to a pulse sequence with 100 percent duty cycle whereas the temperature curve with ripples belongs to a 1 percent duty cycle pulse sequence with TR = 500sec

# Appendix D

# Gradient induced currents on cardiac pacemakers

It is possible to acquire images in MRI, when gradient coils are used with a birdcage coil and in the presence of a main magnetic field. Gradient coils scatter low frequency (on the order of KHz) electromagnetic fields which may cause peripheral nerve stimulation (PNS).

All living cells exhibit a voltage of approximately 90mV across their membrane so called the membrane potential. Nerve and muscle cells have the unique capability of creating short electrical impulses in response to appropriate stimuli. Once the stimulus exceeds a certain strength an impulse is created which propagates along the cells connected to each other. This is the basic principle of nerve stimulation. Using this principle, PNS is used in the localization of nerves for the purpose of peripheral nerve blockade [32].

In an MR scanners, the field created by the gradient coils may stimulate nerves by induction. At the presence of an implant in the body, a pacemaker in our case, such a stimulation is more likely since the field is amplified. In this section, the gain in electric field at the tip of the pacemaker lead due to gradient coils is investigated.

*Pacemaker model*

The case of the pacemaker is 0.8 mm thick. On y-z plane, the case is modelled by the combination of a 5 trapezoid (on top) with a half ellipse (bottom) having an elliptic ratio of 0.7. The short top side of the trapezoid is 4 cm and the long bottom side is 5 cm. The distance in between is 2 cm.

The wire is connected to a spot that is 1.25 cm from the upper-left corner of the case, it goes up 1 cm, turns right until it is on the same level with the upper-right corner of the case. Than the lead takes one tour around the case. It is directly connected to the case since this is the worst case situation in terms of heating. After one tour around the case, another half ellipse with 0.7 elliptic ratio is travelled. Now we are 5 cm away from the right top corner of the case. Than the wire goes 11 cm downward and makes a quarter circle of radius 2 cm.

The wire diameter is 0.8 mm and the coating thickness is 0.35 mm. Relative insulation permittivity is 2.3. 5 mm at the tip of the lead is left uninsulated. Total length of the lead is 45 cm.

Tissue properties at low frequencies very different. At these frequencies permittivity values goes up by several orders and conductivity is not very different than MHz range . Accordingly, conductivity was taken to be 0.5 S/m and the relative permittivity was taken to be 1000000 according to the plots given by AFRL[33].

A simulation is performed with the pacemaker model that is very similar to mentioned previously (materials and methods section), at 1 KHz. Incident electric Field at the location of the pacemaker was 1 V/m (Ez), And it was amplified by an amount of 90 due to the presence of the implant, indicating the probability of nerve stimulation in this region.

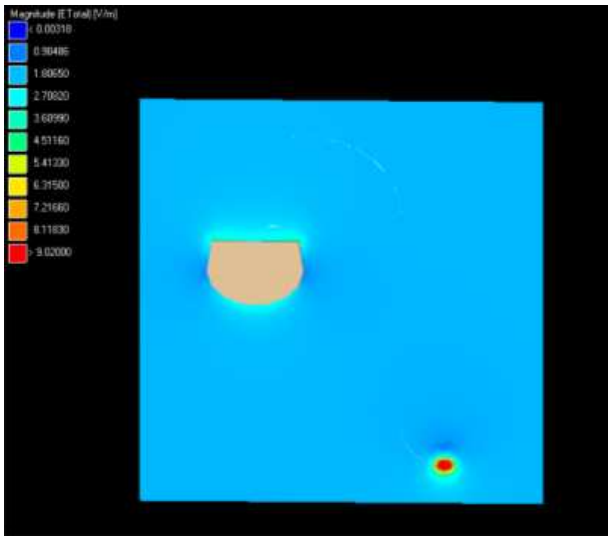


Figure D.1: Maximum amplification in the electric field is at the tip